Journal of Magnetic Resonance 300 (2019) 8–17

Contents lists available at ScienceDirect

Journal of Magnetic Resonance

journal homepage: www.elsevier.com/locate/jmr

High-throughput continuous-flow system for SABRE hyperpolarization

Petr Štěpánek [a,*], Clara Sanchez-Perez [b,1], Ville-Veikko Telkki [a], Vladimir V. Zhivonitko [a], Anu M. Kantola [a,*]

[a] NMR Research Unit, Faculty of Science, University of Oulu, P.O. Box 3000, FI-90014, Finland
[b] Environmental and Chemical Engineering, Faculty of Technology, University of Oulu, FI-90014, Finland

ARTICLE INFO

Article history:
Received 12 December 2018
Revised 9 January 2019
Accepted 10 January 2019
Available online 14 January 2019

Keywords:
Hyperpolarization
NMR spectroscopy
SABRE
para-H_2
MRI
Flow imaging

ABSTRACT

Signal Amplification By Reversible Exchange (SABRE) is a versatile method for hyperpolarizing small organic molecules that helps to overcome the inherent low signal-to-noise ratio of nuclear magnetic resonance (NMR) measurements. It offers orders of magnitude enhanced signal strength, but the obtained nuclear polarization usually rapidly relaxes, requiring a quick transport of the sample to the spectrometer. Here we report a new design of a polarizing system, which can be used to prepare a continuous flow of SABRE-hyperpolarized sample with a considerable throughput of several millilitres per second and a rapid delivery into an NMR instrument. The polarizer performance under different conditions such as flow rate of the hydrogen or liquid sample is tested by measuring a series of NMR spectra and magnetic resonance images (MRI) of hyperpolarized pyridine in methanol. Results show a capability to continuously produce sample with dramatically enhanced signal over two orders of magnitude. The constant supply of hyperpolarized sample can be exploited, *e.g.*, in experiments requiring multiple repetitions, such as 2D- and 3D-NMR or MRI measurements, and also naturally allows measurements of flow maps, including systems with high flow rates, for which the level of achievable thermal polarization might not be usable any more. In addition, the experiments can be viably carried out in a non-deuterated solvent, due to the effective suppression of the thermal polarization by the fast sample flow. The presented system opens the possibilities for SABRE experiments requiring a long-term, stable and high level of nuclear polarization.

1. Introduction

Nuclear magnetic resonance (NMR) is an invaluable method finding applications in many fields ranging from physics through chemistry to biological studies. It is a very versatile technique, offering ways for elucidation of complex molecular structures [1], measuring dynamic molecular processes [2] or investigating porosity of materials [3]. Moreover, it forms a basis of magnetic resonance imaging (MRI), an indispensable tool in contemporary medical diagnosis and a generally versatile method for non-invasive visualization of spatial density of atomic nuclei.

The broad impact of NMR and MRI was achieved despite their rather poor signal strength. The NMR signal acquired during the experiment is directly proportional to the difference in populations of the spin states of the observed nuclei. In a traditional experiment at thermal equilibrium, the spin state populations are governed by Boltzmann distribution, which is a function of temperature and the strength of the magnetic field the sample is subjected to. At ambient temperatures the population differences between spin states achievable in such way are only on the order of 10^{-5}, even when strong magnetic fields of several Tesla are used. Consequently, the development of methods for increasing the spin polarization has received a significant attention.

In order to boost the NMR signal, several methods have been devised. These so-called hyperpolarization (HP) techniques can increase the nuclear spin polarization beyond the thermal equilibrium state, often by several orders of magnitude. The HP process uses an external source of spin order that is transferred to the sample and creates large differences in spin-state populations. The relative population differences as high as tens of percent have been achieved [4–7]. However, unless the spin order is converted to a long lived state [8], the hyperpolarized samples usually readily relax towards thermal equilibrium populations, constraining the usable lifetime of the magnetization.

In one HP method, dynamic nuclear polarization (DNP) [5], the nuclei are polarized using unpaired electrons from free radicals.

* Corresponding authors.
E-mail addresses: petr.stepanek@oulu.fi (P. Štěpánek), clara.sanchezperez@oulu.fi (C. Sanchez-Perez), ville-veikko.telkki@oulu.fi (V.-V. Telkki), vladimir.zhivonitko@oulu.fi (V.V. Zhivonitko), anu.kantola@oulu.fi (A.M. Kantola).
[1] Present address: Department of Chemistry, University College London, 20 Gordon Street London WC1H 0AJ, United Kingdom.

https://doi.org/10.1016/j.jmr.2019.01.003
1090-7807/

DNP is a very versatile method, capable of polarizing a wide range of molecules. However, it requires very expensive facilities, has high operational costs and the repeatability of the level of polarization may be difficult to predict.

Another HP method is spin-exchange optical pumping (SEOP) [6], in which polarization is transferred from electrons of vaporized alkali metal atoms to noble gas nuclei. The SEOP process can achieve a very high degree of polarization, up to 90% [9], but it is in practice usable only for polarizing of noble gas atoms, such as helium, xenon or krypton [10].

Lastly, a number of hyperpolarization methods, called parahydrogen induced polarization (PHIP) [6], use parahydrogen (*para*-H_2, one of the spin isomers of hydrogen) as the source of the spin order. In some PHIP approaches, *para*-H_2 can be directly incorporated into the molecule via addition reaction with a suitable unsaturated bond, producing molecules with non-equilibrium spin populations in schemes known as PASADENA [11,12] or ALTADENA [13].

Recently, it has been shown that PHIP can also be used to transfer the magnetization from *para*-H_2 to the hyperpolarized molecules without actual chemical modification taking place. Such effect can be achieved by a reversible association of the substrate molecule with *para*-H_2 mediated by a suitable metal catalyst. The technique is known as Signal Amplification By Reversible Exchange (SABRE) [14]. The SABRE polarization mechanism is based on the transfer of spin order via the scalar couplings of the *para*-H_2 and the substrate molecule, and its efficiency depends on the strength of the magnetic field in which the polarization transfer takes place, so-called polarization transfer field (PTF) [14–18]. Protons are most efficiently polarized in the field of several mT, but in the case of heteronuclei, very low fields on the order of μT are optimal, requiring magnetic shielding from the Earth's natural magnetic field [19–22]. While SABRE is not as versatile as, *e.g.*, DNP [5,7], it is nevertheless capable of hyperpolarizing a significant range of nuclei and molecular substrates, provided that they can associate with the polarization-transferring Ir catalyst. Moreover, its costs for instrumentation facilities are orders of magnitude smaller than for DNP, making it an affordable hyperpolarization option. In addition, since SABRE does not modify its substrate, it can be used to produce stable, predictable levels of nuclear spin polarization in a continuous fashion, as has been shown [23–37].

Since the first description of SABRE, a number of significant developments have been made. Following the initial report [14], which used [Ir(COD)(py)(PCy_3)][BF_4] (COD = cyclooctadiene, py = pyridine, PCy_3 = tri-cyclohexyl-phosphine), synthetic efforts yielded more potent catalysts allowing more efficient polarization transfer or solvent compatibility [15,17,38–41]. Currently, one of the most efficient SABRE catalysts is of the general form [Ir(IMes)$(L)_3(H_2)$] (IMes = 1,3-bis(2,4,6-trimethylphenyl)-imidazolium, L is a ligand molecule, not necessarily identical in all three coordination places). It is an activated form of an air-stable precursor [Ir(COD)(IMes)]Cl, which can be in turn readily prepared from commercial reagents [42,43].

Apart from protons (see, *e.g.*, [14,16,44–46]), other nuclei such as ^{13}C [18,24,25,44,47], ^{15}N [20–22,30,41,44,45,48–50], ^{19}F [14,51,52], ^{31}P [19,53], ^{29}Si [54] and ^{119}Sn [54] have been successfully polarized. The SABRE polarization transfer has also been achieved in high magnetic fields [28,31,55,56] and the suitability of the SABRE for 2D NMR techniques [57–59], low concentration detections [46] and imaging [14,21,25,29,47,51,53,60–62] has been demonstrated as well. In addition to the NMR measurements in high-field instruments, the SABRE has also been successfully used in low-field set-ups [25,47,63], where use of hyperpolarized samples yields even more pronounced results due to the much smaller achievable thermal polarization. The issue of contaminating the sample with the SABRE catalyst can be overcome by immobilization of the catalyst on solid support [49,64,65] or via extraction of the analyte using two-phase system of immiscible liquids [66].

The first experimental approach to SABRE, which is still in use today, is a manual shaking of the sample under *para*-H_2 atmosphere inside a pressurized valved NMR tube to introduce the hydrogen gas into the solution. After thorough mixing the sample is immediately inserted into NMR spectrometer for measurement. Since the relaxation is one of the crucial parameters affecting the efficiency of the technique, an effort has been directed towards instrumentation that would shorten the delivery time of the sample. One such approach is an automated computer-controlled flow system with pre-polarizing magnet and a flow probehead, which allowed for repeatable preparation and transfer of hyperpolarized sample into NMR spectrometer by applying gas pressure [15,24]. Such system allows to polarize the same sample multiple times by cycling it between the NMR probe and the polarizer where it is periodically repolarized. Another option is an automated mechanical shuttling of the whole sample using a motorized system [67,68]. One can also use a continuous *in situ* polarization without transfer of the sample. The approach has been shown either in low field setup of several mT [25–27,29], simultaneously exploiting the favorable conditions for ^1H SABRE transfer, or in high fields [30–32]. The experiments can be performed either with stopping of the flow of *para*-H_2 before individual acquisitions [32–34] or with the constant flow of *para*-H_2 at all times, even during measurement time, creating a truly continuous polarization [27,28,35–37]. Yet another method, a continuous flow system using a membrane reactor has been described recently [69] and its features are compared with the setup presented in this paper in the Results section.

Here we present a different approach to sample preparation and transfer based on a continuously flowing liquid. Our system is inherently well-suited for flow imaging and delivers a steady flow of sample with a stable level of nuclear spin-polarization. It also provides a high throughput of the sample on the order of millilitres per second. We describe the overall system, its main components and features and discuss its performance parameters, such as the influence of the pumping speed of liquid, influx of hydrogen gas and polarization transfer field strength and their influence on the signal strength. We focus mainly on the unique features of our system, such as flow rates and efficiency of the hydrogen exchange with the liquid phase. The details of kinetic aspects of the SABRE in solution have been discussed extensively in the literature before (see, *e.g.*, [24] and references cited therein) and it is reasonable to assume they are preserved irrespective of the mode of sample preparation and transportation into the spectrometer.

2. Methods

2.1. Polarizer overview

The overall schematic of the system is presented in Fig. 1. The main parts of the setup are: high pressure hydrogen cylinder (A), custom made *para*-H_2 converter (B), low-field electromagnet (C), vacuum pump (G), peristaltic pump for sample (I), and main framework with tubing, valves and polarizing vessel. The main body of the polarizer is fixed onto a plexiglass (see Fig. S1 in Supporting Information for full view).

2.2. Principle of operation

The system allows for several modes of operation. After introducing the sample into the degassing compartment (H), a vacuum

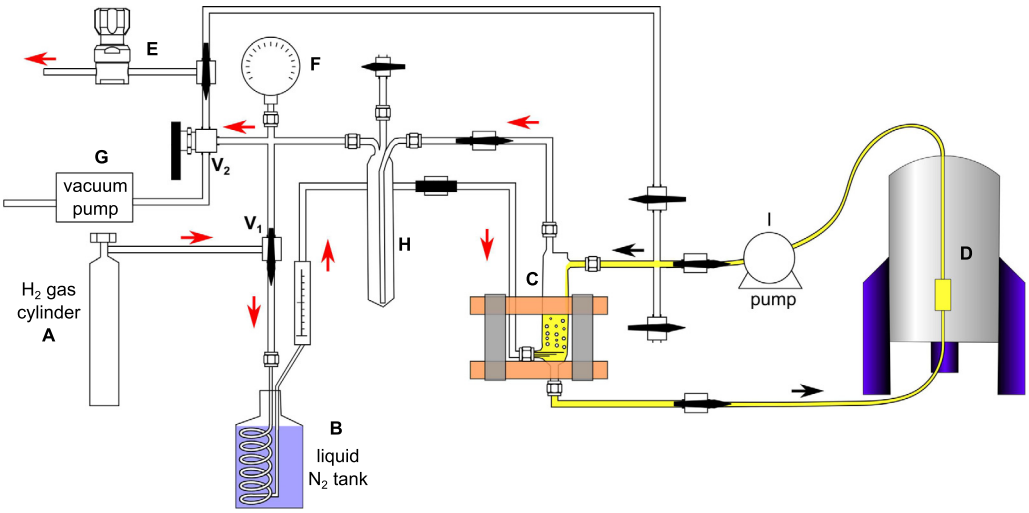

Fig. 1. Overview of the continuous flow SABRE polarizer: The hydrogen gas from a gas cylinder (A) is cooled down to 77 K and converted to 50% *para*-H_2 using FeO(OH) in a custom hydrogen converter (B). The *para*-H_2 enriched gas bubbles up through the liquid sample, which is being pumped in the opposite direction (downwards, assisted by the gravity) between the polarizing cell (C) inside an electromagnet coil and the NMR spectrometer (D). Excess hydrogen escapes through back-pressure regulator (E) maintaining a stable pressure inside the system, which can be monitored via the pressure gauge (F). Prior to the experiment, vacuum pump (G) is used for degassing of the sample inside the degassing compartment (H) before transferring it to the polarizing cell. For this purpose, two three-way valves V_1 and V_2 are used to redirect the flow of hydrogen and connect the system to either vacuum pump or back-pressure regulator, respectively. Red arrows symbolize flow of hydrogen gas and black arrows represent the flow of liquid sample during operation. (For interpretation of the references to colour in this figure legend, the reader is referred to the web version of this article.)

pump can be used to degas the sample via the freeze-pump-thaw cycle. The sample is then transferred to the polarizing cell by applying slight overpressure into the degassing vessel via the three-way valve V_1. During the polarization operation the hydrogen gas passes through the converter immersed in liquid N_2 (B), where it is enriched to 50% *para*-H_2 by conversion over FeO(OH), and flows through the sample in the polarizing cell (C). The hydrogen is introduced into the sample in polarizing cell via three 1/16 inch thick pieces of tubing. The gas flow is regulated by a needle valve and monitored by a flow-meter. The valve V_2 allows to reroute the connection from vacuum pump to back-pressure regulator and maintain a stable pressure inside the whole system even as new *para*-H_2 flows constantly in. Pressure of up to 7 bar has been successfully tested.

The liquid sample is pumped independently of the hydrogen flow via the peristaltic pump. The pump is placed in the line after the NMR spectrometer in order to minimize travel time from cell to spectrometer (connected via 2.4 m long tubing, corresponding to less than two seconds travel time at the highest speed) and hence the loss of polarization due to the relaxation. The pumping direction can be chosen freely, but pumping the liquid in downward direction opposite to the flow of the rising hydrogen bubbles provides better mixing of the sample, allows the freshest incoming *para*-H_2 to be in contact with the sample immediately leaving the polarizing cell and minimizes probability of stray bubbles to enter the sample. Moreover, it also allows using a smaller amount of sample. After passing through the NMR spectrometer, the sample is returned to the cell for refreshing of the polarization.

During the experiment the degassing vessel (H) can be used as a solvent trap by immersing it in cold bath in order to condense escaping solvent vapours, which can be then periodically returned back to maintain a stable sample volume.

2.3. Sample preparation

The sample solutions consisting of methanol (non-deuterated), pyridine and [Ir(IMes)(py)$_3$(H$_2$)] were degassed prior to measurements. Pyridine was chosen as one of the most well-studied molecules in SABRE. The first portion of the sample was prepared by dissolving 180 µl (2.25 mmol) of pyridine in 45 ml of methanol and transferred to the polarizing cell. The second portion of the sample was prepared by dissolving 180 mg of IMes catalyst in 20 ml of methanol and subsequent addition of 80 µl (1 mmol) of pyridine. The second solution thus had identical concentration 50 mmol/l of pyridine as in the first batch, allowing us to make a titration with the catalyst while maintaining constant concentration of pyridine. The titration was performed in four steps, each time transferring 5 ml of the catalyst solution from the degassing vessel to the polarizing cell and mixing thoroughly. The four samples yielded concentrations 1.4, 2.6, 3.5 and 4.3 mmol/l of catalyst and were labelled c_1 to c_4 in order of increasing concentration, corresponding to ratios of catalyst to pyridine 1:35, 1:20, 1:14 and 1:12.

The total methanol loses during the degassing steps were measured as a decrease in level of the liquid surface in the degassing vessel and are estimated to be under 1 ml and thus not significant, given the total sample volume (varied between 45 and 65 ml).

Unless otherwise stated, the flow rate of hydrogen was set to 0.9 ml/s, flow rate of the sample to 170 ml/min and hydrogen gas pressure to 5 bar.

2.4. NMR measurements

All the NMR and MRI experiments were performed on Bruker AVANCE III 300 spectrometer equipped with micro-imaging unit, using Micro 2.5 probe with a 25 mm birdcage coil tunable for ^{1}H.

The sample was flowing through a straight piece of perfluoroalkane (PFA) tubing (outer diameter 6.35 mm (1/4 inch), inner diameter 3.96 mm (0.156 inch), Swagelok). PFA tubing was fixed concentrically with the coil axis by a 3D printed PET (polyethylene terephthalate) holder. The proton NMR spectra on the straight PFA tubing were recorded with one scan using a 45 deg pulse.

As our interest in the present study was focused on hyperpolarized signals of pyridine and methanol, we left the hydride signals of SABRE catalyst outside the spectral width. Their presence was confirmed in our preparatory SABRE experiments.

2.5. MRI measurements

MR images were recorded either for the identical tubing as was used for NMR experiments or for a phantom flow channel created

by connecting two pieces of PFA tubing of different inside diameters (3.2 and 3.96 mm) by a nylon compression fitting with inside diameter of 4.8 mm (see Fig. S2 in SI for details). The fitting was fixed in the center of the probe using a padding constructed from extruded polystyrene. Due to the shape of the resulting object, the shimming proved to be rather difficult, and the field inhomogeneity gave rise to broad baseline (Fig. S3 in SI). This prohibited use of selective pulses as excitations targeting the pyridine region would also excite a non-negligible portion of methanol nuclei. For this reason, the images were recorded using hard pulses covering the whole spectral region of interest, including both methanol and pyridine, and the individual component intensities were obtained by subtraction.

The 2D spin density images in the straight PFA tubing were measured using a gradient echo sequence with first order flow compensation. The images were recorded with an echo time, T_E, of 12.3 ms and repetition time, T_R, of 50 ms. The signal of interest (pyridine or methanol) was exited using a selective Hermitian pulse with an excitation bandwidth of 270 Hz. The slices were oriented in the plane of the tube axis, with thickness 2 mm, the field of view (FOV) 20×20 mm, and a resolution of 156 μm/pixel on the 2D plane. For each image 128 averages, N_{av}, were collected (experimental time ca. 14 min).

The 2D flow images were recorded using the velocity encoded gradient-echo provided by the Paravision 5.1 software (Bruker BioSpin). Bipolar gradients were used to produce a phase shift proportional to the velocity, thus encoding the velocity distribution of the moving spins into each pixel made by the two spatial dimensions (read and phase directions). In the Fourier flow mapping mode used in this work, two encoding steps were required to velocity encode one main spatial (vertical) direction. The experiments on the phantom constructed from the fitting and tubings were recorded using the following parameters: $T_E = 2.1$ ms, $T_R = 10.6$ ms, $N_{av} = 200$, FOV = 20×20 mm (resolution of 156 μm/pixel in the 2D plane), and slice thickness 1.25 mm. The slices were oriented along the axis of the tubing. The maximum velocity and the velocity resolution for the flow encoding were 80 cm/s and 10 cm/s, respectively (experimental time ca. 54 min).

3. Results and discussion

All numerical NMR data are reported as signal enhancements of NMR peaks with respect to the signal of fully thermally polarized sample in 300 MHz (7 T) magnet (see SI for details). Specific ranges for integration are given in Table S1 in SI. Note that in the flowing sample the signal of methanol is dramatically reduced due to the short time period spent in the field before being introduced into the probe, significantly reducing the thermal polarization.

3.1. Effect of the flow rate on the signal amplitude

The first set of experiments demonstrates the effect of different flow rates of the sample from polarizing cell to the NMR spectrometer. We have measured NMR spectra in the region of flow rates from 0 to 170 ml/min in steps of 17 ml/min for each sample c_1 to c_4. The results are plotted in Fig. 2. We note that the flow rate is considerably higher than 10 ml/min of the previously reported continuous flow system [69]. This allows for new applications where a large volume of sample would be required, such as imaging of larger flow channels. It, however, also requires somewhat larger sample volume of 50 ml, compared to 30 ml in Ref. [69], in order to assure sufficient time in the reactor for the polarization transfer to take place.

The first apparent trend is the steadily increasing observed magnitude of the hyperpolarized (HP) signal with the flow rate. This is an interesting contrast to the continuous flow system in [69], where an optimal flow rate was found below its maximum value. The likely cause are different methods of mass transfer of hydrogen into the solution in the two systems, which influence the kinetics of SABRE transfer. An interesting point is that at slower speeds the lowest concentration of catalyst seems to provide the largest enhancement, while samples with increasing catalyst loadings provide progressively smaller enhancement. On the other hand, higher catalyst loadings achieve larger enhancement at higher flow rates (faster delivery speeds). In addition, the maximum achieved enhancement, while not significantly dependent on the catalyst concentration, is the largest for the medium catalyst loadings.

Since faster delivery speeds offer higher HP signal, the trends suggest that proton relaxation, rather than the reaction kinetics associated with the spin-transfer, is the key factor influencing the observed signal intensity. While the SABRE catalyst builds up the sample polarization over time, it also shortens the effective relaxation time of pyridine [24]. At low catalyst concentrations the loss of polarization due to this effect is diminished owing to the lesser probability of association of hyperpolarized pyridine with the scarce catalyst molecules. On the other hand, higher catalyst concentrations offer higher reaction throughput, leading to increased HP signal when the flow rates are high enough to offset the shortened relaxation times. However, at the highest catalyst loading the effect of the fast relaxation seems to start to overcome even the fastest delivery once again (sample c_4).

A new signal appears at ca. 4.5 ppm, which can be assigned to hyperpolarized dissolved hydrogen gas [55] (see also Fig. S4 in SI). This signal is not apparent in the thermally polarized sample. As documented throughout Figs. 2–6, the signal depends on a number of system parameters and increases in concert with the pyridine protons, underlining its origin due to the SABRE hyperpolarization process.

As another representation, the enhancements of the proton signals are plotted in Fig. 3 for each individual signal, showing rather limited effect of the catalyst concentration and more clearly demonstrating the highest polarization for concentration c_3.

The maximum obtained signal enhancement (as a ratio of integrated hyperpolarized signal to the thermal one in 300 MHz magnet) in this set of experiments is 105 for the sample c_3, corresponding to the polarization of about 0.25%. Full table of values is given in SI (Table S2).

3.2. Effect of the hydrogen flow rate on the signal amplitude

The second set of experiments consisted of measuring the dependence of signal strength on the hydrogen flow. With increasing flow, one to three independent streams of bubbles form from the three capillaries and ascend through the solution, dissolving *para*-H_2 enriched gas into the liquid while also mixing the solution. We performed three separate measurements at flow rates of 0.5, 0.9, or 1.8 ml/s. The results are shown in Fig. 4.

It is apparent that at the lowest catalyst loading, the effect of hydrogen flow rate is quite limited. At such low concentration the catalyst availability is likely the rate determining step and the additional *para*-H_2 gas thus has a limited impact. Following the trend of the lowest *para*-H_2 flow rate across different concentrations (red[2] bars), we see that the SABRE efficiency slightly decreases with higher catalyst loadings. This effect is likely due to the fact that at higher concentrations there is not enough fresh *para*-H_2 to bind to the abundant catalyst for new polarization transfer, but

[2] For interpretation of color in Fig. 4, the reader is referred to the web version of this article.

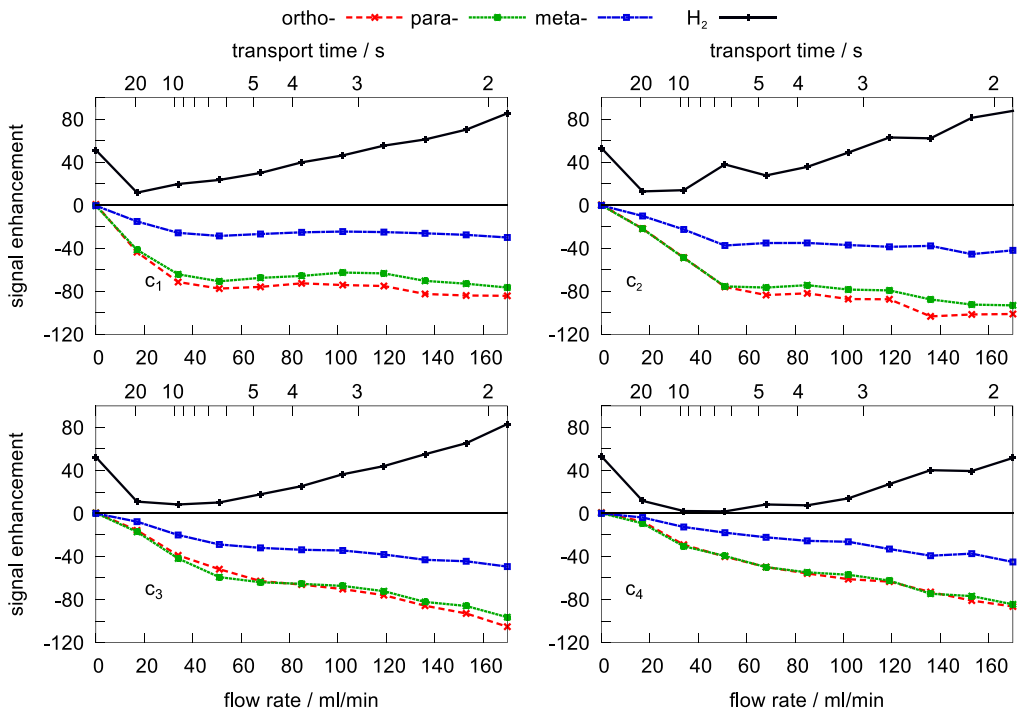

Fig. 2. The comparison of dependence of observed NMR signals on catalyst concentration and sample flow rates expressed as relative enhancement compared to thermally polarized signal at 7 T. Catalyst concentrations are $c_1 = 1.4, c_2 = 2.6, c_3 = 3.5, c_4 = 4.3$ mmol/l. The large value of H_2 at low flow rate comes from the tailing of the large thermally polarized methanol signal into the integration region (see also Fig. S4 in SI).

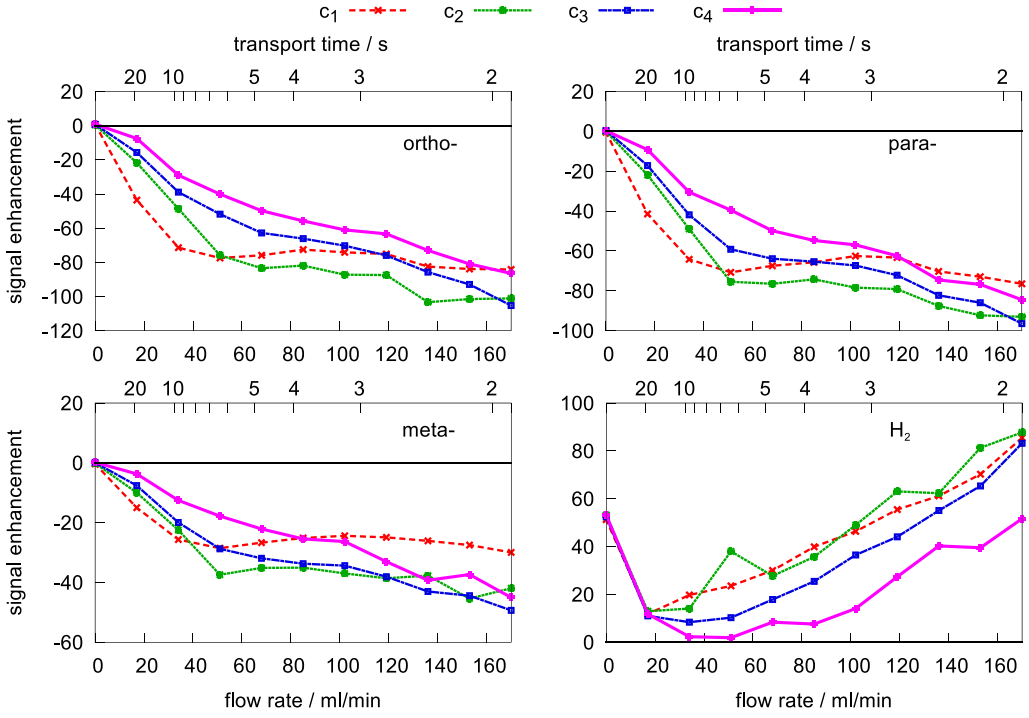

Fig. 3. The comparison of dependence of observed NMR signals on catalyst concentration and sample flow rate grouped by individual proton sites. The concentrations increase in the order $c_1 = 1.4, c_2 = 2.6, c_3 = 3.5, c_4 = 4.3$ mmol/l as red, green, blue, magenta. The large value of H_2 at low flow rate comes from the tailing of the large thermally polarized methanol signal into the integration region (see also Fig. S4 in SI). (For interpretation of the references to colour in this figure legend, the reader is referred to the web version of this article.)

the additional catalyst instead shortens the effective relaxation time. On the other hand at higher *para*-H_2 influx, more catalyst molecules can bind with the now available *para*-H_2 and increase the polarization, which is reflected as a progressively higher dependence of the HP signal amplitude on the gas influx at the medium flow rates (green). In this case the achieved polarization increases from c_1 to c_3 and drops off only at c_4. At the highest *para*-H_2 flow rate the polarization dependence on the concentration does not decrease significantly even at c_4, consistently with our hypothesis. In summary, there appears to be a delicate balance between the *para*-H_2

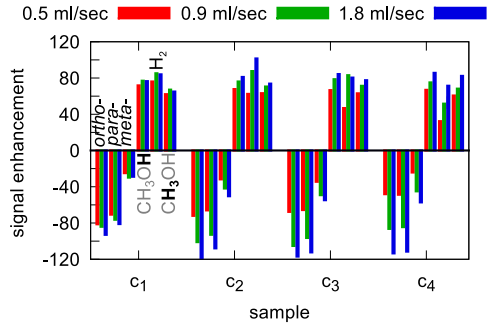

Fig. 4. The effect of flow rate of hydrogen bubbling through the solution on the NMR signal intensity. The six signals correspond to protons in *ortho-*, *para-*, *meta-* position of pyridine, hydroxyl proton of methanol, polarized H_2 and methyl protons of methanol. Note that methanol signals also reflect significant portion of thermally polarized molecules. Moreover, because of very large thermal equilibrium reference signal, their intensities are multiplied by 1000 for visibility. The concentrations of SABRE catalyst increase in the order $c_1 = 1.4, c_2 = 2.6, c_3 = 3.5, c_4 = 4.3$ mmol/l.

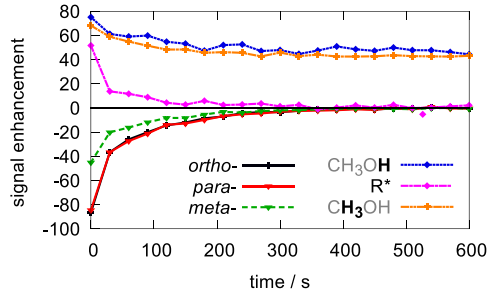

Fig. 5. The time evolution of the integrated NMR signals after stopping the hydrogen influx at $t = 0$ (sample $c_4 = 4.3$ mmol/l). The six signals correspond to protons in *ortho-*, *meta-*, *para-* position of pyridine, hydroxyl proton of methanol, polarized H_2 and methyl protons of methanol. Note that methanol signals approach intensity corresponding to partially thermally polarized molecules, and their intensities are multiplied by 1000 for visibility.

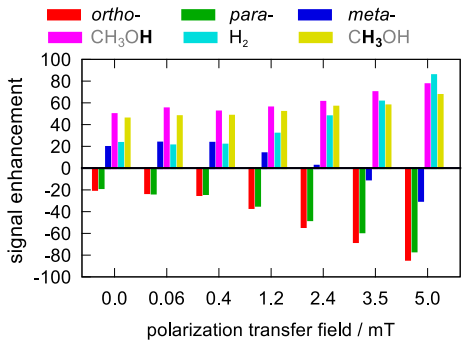

Fig. 6. The effect of the polarization transfer field on the intensity of the observed NMR signals (sample c_4). The value of 0.06 mT represents the Earth magnetic field plus the fringe field of the magnet when the electromagnet in not powered while the value of 0 corresponds to the active cancellation of these fields by the electromagnet. The six individual signals correspond in order to protons in *ortho-*, *para-*, *meta-* position of pyridine, hydroxyl proton of methanol, polarized H_2 and methyl protons of methanol. Note that methanol signals also reflect significant portion of thermally polarized molecules. Moreover, because of very large thermal equilibrium reference signals, their intensities are multiplied by 1000 for visibility.

flow rate and SABRE catalyst concentration. At low concentrations, the catalyst is the rate determining factor and the superfluous *para*-H_2 is effectively wasted. On the other hand, using insufficient *para*-H_2 flow rate at higher catalyst concentrations does not fully employ the catalyst, which can then contribute more to the relaxation. The largest obtained enhancement in this set of experiments was 119, corresponding to about 0.29% polarization. This polarization compares well with the 0.14% reported in [69], where Earth's magnetic field was used as PTF.

The intensity profile of the signal coming from the hyperpolarized hydrogen at 4.5 ppm is similar to the pyridine signals by being rather insensitive to the *para*-H_2 flow rate at the lowest concentration and increasing only at higher concentrations. Moreover, it can be seen that both proton signals of methanol also respond to the hydrogen flow in a similar way, providing an evidence for slight hyperpolarization of methanol in addition to the thermal contribution coming from transport through the stray fields on the way to the NMR probe. The polarization of solvent by SABRE has been reported before for acetonitrile [18,70], methanol [17,71], ^{15}N in neat pyridine [72], and water was also polarized in a similar way [73]. In our case the total contribution from the SABRE process is rather large, likely because the SABRE experiments are usually conducted in deuterated solvents, in contrast to our proton-rich solvent. Thus, our system contains much more available ^1H nuclei as receivers of the polarization, leading to substantial total increase of the signal. Interestingly, such polarization of methanol has not been observed in previous continuous flow SABRE experiment [69], possibly as an effect of different PTF, which is quite strong in the low mT region [17].

Apart from the bubbles raising through the sample, there is a second interface between the gas and the liquid at the point where the sample returns from the spectrometer to the polarizing cell. The liquid here forms a thin film on the inner wall of the cell and at higher flow rates even splashes through the hydrogen atmosphere. In both cases, a significant interface between the liquid and the gas is created, enabling another way for dissolving hydrogen.

In order to gain some insight into the efficiency of this process, we ran an experiment where at time $t = 0$ the flow of hydrogen was stopped, thus ceasing the creation of the bubbles, but the sample was let to circulate, preserving the gas-liquid interface at the sample-return inlet. An NMR spectrum was taken every 30 s for 10 min with results shown in Fig. 5. As can be clearly seen, an easily discernible hyperpolarization is observed even after several minutes. For comparison, the average time for the whole sample volume to circulate through the system is ca. 23 s. Such long persistence considering short relaxation time of protons leads us to the conclusion that there must be an ongoing process refreshing the polarization of the sample. Since the bubbling can no longer be a contributing factor, the interface at the sample inlet is likely the source of persistent introduction of fresh *para*-H_2 into the sample. As expected, the overall signal intensity gradually decreases over time due to the depletion of the *para*-H_2 atmosphere. In addition, a similar loss of polarization can once again be seen for both methanol protons as well as for H_2 signal.

3.3. Effect of the polarization transfer field strength

It is well established that the efficiency of the SABRE effect is dependent on the strength of the magnetic field which facilitates the polarization transfer, the so-called polarization transfer field (PTF). We explored this effect in our system by measuring the signal strength at several values of PTF produced by the electromagnet outside of the polarizing cell (Fig. 6).

At first glance different behaviour of the *ortho-* and *para-* protons compared to *meta-* can be seen where the former show negative signals insensitive to the low PTF strengths and rapidly increasing in intensity above 0.4 mT. On the other hand signal of *meta-* protons starts as positive peak at zero field and gains a small amount of intensity before rapidly decreasing and switching sign to negative values.

We can also see that the field dependence of the H_2 signal more closely resembles that of the *ortho-* and *para-* hydrogen atoms rather than that of the *meta-* in the sense that it is quite small at low fields, after which it grows rapidly.

Generally the signal increases with higher PTF. Our setup did not allow to test stronger fields than those reported in Fig. 6. In the future, the setup could be upgraded with the coils allowing stronger PTF and, therefore, potentially higher polarization degree.

3.4. Spin density imaging

As a test of the imaging capabilities of the system, we acquired a set of FLASH images of the sample flowing through the tubing (Fig. 7). The images were recorded using selective excitation pulses (see Methods section) on either the pyridine or methanol signal. As can be seen, under the given conditions no signal can be discerned in the image of thermally polarized pyridine. On the other hand, hyperpolarized pyridine produces a strong signal, clearly showing the sample inside the tubing. The signal is even stronger than that from the thermally polarized methanol, which is in large excess in comparison to the pyridine (concentration of pure methanol is 24.7 mol/l, while the pyridine concentration is 50 mmol/l, a ratio of almost 300 when accounted for number of protons per molecule).

An interesting note is the spin density profile across the tubing diameter. As seen in the lower panel of Fig. 7, methanol produces stronger signal near the edges of the tubing, while the pyridine signal is strongest in the center. This is readily explained by the origin of the spin magnetization - a significant portion of the methanol nuclei is polarized thermally, which means that the longer they stay inside the magnet, the stronger signal they will produce. Since the slowest liquid layers are found near the wall of the tubing, the spins in these volume elements spend longer time in the field and acquire higher thermal polarization than the ones closer to the center of the tube. In the case of pyridine the situation is reversed as practically all signal comes from the hyperpolarized nuclei with negligible signal arising from the thermal polarization due to the low concentration of pyridine. Thus, the slower molecules near the walls lose their polarization via relaxation, giving rise to weaker signal compared to the fast flowing fresh hyperpolarized sample in the middle. It is worth pointing out that Fig. 7 shows image of a thin slice from the center of the tubing and the intensity variation is thus not affected by the cylindrical geometry of the tubing.

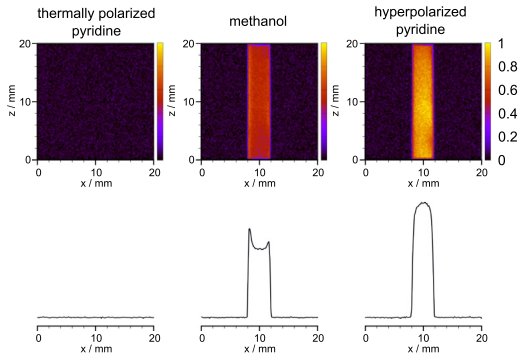

Fig. 7. MR image of the solution flowing in the tubing with selective excitation pulses on pyridine (left and right) or methanol (middle) signals. The bottom part of the figure represents the sum of values from all pixels in each column of the image. The catalyst concentration was 4.3 mmol/l, the sample flow rate was 12 cm/s and the slice thickness 2 mm.

3.5. Velocity mapping

As a second set of imaging experiments, we have performed the velocity mapping on the phantom object (see Methods section and Fig. S2) using FLOWMAP. The phantom was chosen in order to demonstrate different velocities of the sample flowing through channel of changing diameter. One set was recorded with hyperpolarization of the sample and the second set without. The contribution of hyperpolarized pyridine was then obtained as a difference between these two images, bearing in mind that a small contribution from hyperpolarized methanol is likely present. The experiment was run at a single average linear flow rate of 12 cm/s through the tubing. It should be noted, however, that the maximum speed in the center of the tubing can reach higher values during flow. Moreover, the used pump exhibits pulsating flow, giving rise to even faster instantaneous velocities. The distribution of different velocities along the vertical direction is shown in Fig. 8.

As the measured intensity values were rather low, the scale of Fig. 8 is truncated to range 0–30% of maximum intensity to provide larger contrast. Full-scale image can be found in the SI (Fig. S5). A difference can be seen between the second row, corresponding to thermally polarized nuclei - thus, effectively, only the methanol - and the third row, showing difference between thermally polarized and hyperpolarized sample. Near the edges of the tube, particularly in the central, widest part of the channel, the methanol signal clearly dominates in the range of velocities up to 20 cm/s. In the region of 20–50 cm/s the contributions get more even, possibly because the flow is too fast to sufficiently thermally polarize the methanol while also being too slow to retain the hyperpolarization before a significant portion of nuclei relax. In the region of 50–

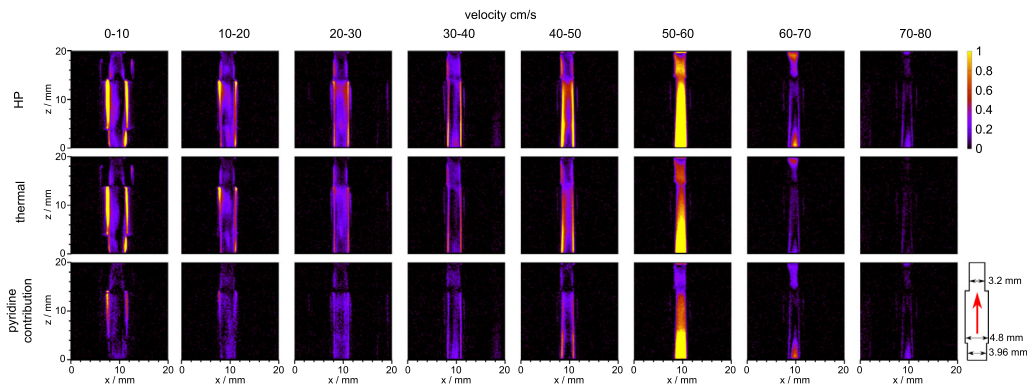

Fig. 8. The velocity profiles of the phantom (shown on the right and in Fig. S2) as measured with (top) and without (middle) hyperpolarizing the pyridine. The lowest segment shows the contribution of pyridine as a difference between the image of hyperpolarized and thermally polarized image. The catalyst concentration was 4.3 mmol/l, the slice thickness 1.25 mm and the average sample flow rate was ca. 12 cm/s (see text for details).

60 cm/s the pyridine nuclei contribute a large portion of the total intensity. At even higher speeds the pyridine is the dominant contributor while methanol is rather weak.

It is apparent that the regions of the slowest velocities, corresponding mostly to methanol, are at the edges of the widest, central region of the phantom. This is expected as the incoming liquid pushes more easily straight through the center of the fitting, leaving the fringes relatively undisturbed. The observed behaviour shows that faster moving liquid carries relatively more pyridine polarization compared to slowly moving regions. This is in general agreement with the previous conclusions from the spin density imaging.

These findings clearly point out the possibility to use hyperpolarized samples to study fast flow rates, that could be impossible to image with non-polarized samples due to lack of time to build up thermal polarization.

4. Conclusion

We have constructed and successfully tested a polarizing instrument for steady production of hyperpolarized samples using the SABRE technique. The system features constantly flowing liquid, which is being continuously mixed with the stream of hydrogen bubbles. A rather high volume of sample required in the current iteration of the instrument can be offset by using a non-deuterated solvent, the signal of which is efficiently suppressed via the insufficient thermal polarization during the flow. Optimization of the delivery tubing to achieve smaller dead volume is also a viable route to improve the issue. The set-up allows a rapid (less than two seconds) introduction of the sample into the NMR instrument for measurements and the tests of the performance show that we are able to obtain over 100 times enhancement of the pyridine signal compared to the fully thermally polarized sample (about 0.29% total polarization). It shall be noted that combined use of a higher polarizing transfer field and more enriched *para*-H_2 gas (up to 3-fold enhancement) and a deuterated solvent could possibly provide up to an order of magnitude higher signal, corresponding to ~3% proton polarization. The increase in signal due to the deuterated solvent would come due to more favourable relaxation and a larger SABRE enhancement of pyridine because of less polarization wasted by transfer to solvent protons.

One of the features of our system is the stability of the delivered polarization, which is not decaying due to the relaxation by virtue of being continuously replaced by fresh sample. In addition, the flow helps to suppress the thermal polarization of the solvent, allowing to perform measurements in normal non-deuterated solvents, signals of which are diminished to about 7% compared to the full thermal polarization. In addition, the bulk methanol solvent is slightly polarized by SABRE, leading to increase of its signal by about 50% as compared to the thermal polarization during the flow. The system design is very suitable not only for NMR spectroscopy and MRI, but also for flow imaging.

Acknowledgement

This project has received funding from the European Union's Horizon 2020 research and innovation programme under the Marie Skłodowska-Curie grant agreement NMOSPEC No 654967 (PS) and from Academy of Finland (Grant 316180) (PS). We acknowledge the generous support provided by the European Research Council (ERC) under Horizon 2020 (H2020/2018-2022/ERC grant agreement No. 772110) and the Academy of Finland (Grant Nos. 289649 and 294027). We also thank the Magnus Ehrnrooth Foundation for financial support (PS). The authors acknowledge financial support from the Kvantum institute (University of Oulu). We are grateful to Anne Selent for the visual documentation of the experiments.

Appendix A. Supplementary material

Supplementary data associated with this article can be found, in the online version, at https://doi.org/10.1016/j.jmr.2019.01.003.

References

[1] J. Keeler, Understanding NMR Spectroscopy, John Wiley & Sons, 2010.
[2] P.T. Callaghan, Translational Dynamics and Magnetic Resonance, Oxford University Press, 2011.
[3] J. Kärger, D.M. Ruthven, D.N. Theodorou, Diffusion in Nanoporous Materials, John Wiley & Sons, 2012.
[4] P.J. Rayner, M.J. Burns, A.M. Olaru, P. Norcott, M. Fekete, G.G.R. Green, L.A.R. Highton, R.E. Mewis, S.B. Duckett, Delivering strong ^{1}H nuclear hyperpolarization levels and long magnetic lifetimes through signal amplification by reversible exchange, Proc. Natl. Acad. Sci. U. S. A. 114 (16) (2017) E3188–E3194, https://doi.org/10.1073/pnas.1620457114.
[5] J.H. Ardenkjær-Larsen, B. Fridlund, A. Gram, G. Hansson, L. Hansson, M.H. Lerche, R. Servin, M. Thaning, K. Golman, Increase in signal-to-noise ratio of >10,000 times in liquid-state NMR, Proc. Natl. Acad. Sci. U. S. A. 100 (18) (2003) 10158–10163, https://doi.org/10.1073/pnas.1733835100.
[6] D.A. Barskiy, A.M. Coffey, P. Nikolaou, D.M. Mikhaylov, B.M. Goodson, R.T. Branca, G.J. Lu, M.G. Shapiro, V.-V. Telkki, V.V. Zhivonitko, I.V. Koptyug, O.G. Salnikov, K.V. Kovtunov, V.I. Bukhtiyarov, M.S. Rosen, M.J. Barlow, S. Safavi, I.P. Hall, L. Schröder, E.Y. Chekmenev, NMR hyperpolarization techniques of gases, Chem. A Eur. J. 23 (2017) 725–751, https://doi.org/10.1002/chem.201603884.
[7] T. Maly, G.T. Debelouchina, V.S. Bajaj, K.-N. Hu, C.-G. Joo, M.L. Mak-Jurkauskas, J.R. Sirigiri, P.C.A. van der Wel, J. Herzfeld, R.J. Temkin, R.G. Griffin, Dynamic nuclear polarization at high magnetic fields, J. Chem. Phys. 128 (2008), https://doi.org/10.1063/1.2833582 (art. no 052211).
[8] M.H. Levitt, Singlet nuclear magnetic resonance, Annu. Rev. Phys. Chem. 63 (2012) 89–105, https://doi.org/10.1146/annurev-physchem-032511-143724.
[9] P. Nikolaou, A.M. Coffey, L.L. Walkup, B.M. Gust, N. Whiting, H. Newtond, S. Barcus, I. Muradyan, M. Dabaghyan, G.D. Moroz, M.S. Rosen, S. Patz, M.J. Barlow, E.Y. Chekmenev, B.M. Goodson, Near-unity nuclear polarization with an opensource Xe-129 hyperpolarizer for NMR and MRI, PNAS 110 (35) (2013) 14150–14155, https://doi.org/10.1073/pnas.1306586110.
[10] D.M.L. Lilburn, G.E. Pavlovskaya, T. Meersmann, Perspectives of hyperpolarized noble gas MRI beyond ^{3}He, J. Magn. Reson. 229 (2013) 173–186, https://doi.org/10.1016/j.jmr.2012.11.014.
[11] C.R. Bowers, D.P. Weitekamp, Parahydrogen and synthesis allow dramatically enhanced nuclear alignment, J. Am. Chem. Soc. 109 (18) (1987) 5541–5542, https://doi.org/10.1021/ja00252a049.
[12] T.C. Eisenschmid, R.U. Kirss, P.P. Deutsch, S.I. Hommeltoft, R. Eisenberg, J. Bargon, R.G. Lawler, A.L. Balch, Para hydrogen induced polarization in hydrogenation reactions, J. Am. Chem. Soc. 109 (26) (1987) 8089–8091, https://doi.org/10.1021/ja00260a026.
[13] M.G. Pravica, D.P. Weitekamp, Net NMR alignment by adiabatic transport of parahydrogen addition products to high magnetic field, Chem. Phys. Lett. 145 (4) (1988) 255–258, https://doi.org/10.1016/0009-2614(88)80002-2.
[14] R.W. Adams, J.A. Aguilar, K.D. Atkinson, M.J. Cowley, P.I.P. Elliott, S.B. Duckett, G.G.R. Green, I.G. Khazal, J. López-Serrano, D.C. Williamson, Reversible interactions with para-hydrogen enhance NMR sensitivity by polarization transfer, Science 323 (2009) 1708–1711, https://doi.org/10.1126/science.1168877.
[15] M.J. Cowley, R.W. Adams, K.D. Atkinson, M.C.R. Cockett, S.B. Duckett, G.G.R. Green, J.A.B. Lohman, R. Kerssebaum, D. Kilgour, R.E. Mewis, Iridium N-heterocyclic carbene complexes as efficient catalysts for magnetization transfer from para-hydrogen, J. Am. Chem. Soc. 133 (2011) 6134–6137, https://doi.org/10.1021/ja200299u.
[16] H. Zeng, J. Xu, J. Gillen, M.T. McMahon, D. Artemov, J.-M. Tyburn, J.A. Lohman, R.E. Mewis, K.D. Atkinson, G.G.R. Green, S.B. Duckett, P.C. van Zijl, Optimization of SABRE for polarization of the tuberculosis drugs pyrazinamide and isoniazid, J. Magn. Reson. 237 (2013) 73–78, https://doi.org/10.1016/j.jmr.2013.09.012.
[17] E.B. Dücker, L.T. Kuhn, K. Münnemann, C. Griesinger, Similarity of SABRE field dependence in chemically different substrates, J. Magn. Reson. 214 (2012) 159–165, https://doi.org/10.1016/j.jmr.2011.11.001.
[18] R.E. Mewis, R.A. Green, M.C.R. Cockett, M.J. Cowley, S.B. Duckett, G.G.R. Green, R.O. John, P.J. Rayner, D.C. Williamson, Strategies for the hyperpolarization of acetonitrile and related ligands by SABRE, J. Phys. Chem. B 119 (2015) 1416–1424, https://doi.org/10.1021/jp511492q.
[19] V.V. Zhivonitko, I.V. Skovpin, I.V. Koptyug, Strong ^{31}P nuclear spin hyperpolarization produced via reversible chemical interaction with parahydrogen, Chem. Commun. 51 (2015) 2506–2509, https://doi.org/10.1039/c4cc08115c.
[20] T. Theis, M.L. Truong, A.M. Coffey, R.V. Shchepin, K.W. Waddell, F. Shi, B.M. Goodson, W.S. Warren, E.Y. Chekmenev, Microtesla SABRE enables 10%

nitrogen-15 nuclear spin polarization, J. Am. Chem. Soc. 137 (2015) 1404–1407, https://doi.org/10.1021/ja512242d.
[21] M.L. Truong, T. Theis, A.M. Coffey, R.V. Shchepin, K.W. Waddell, F. Shi, B.M. Goodson, W.S. Warren, E.Y. Chekmenev, ^{15}N hyperpolarization by reversible exchange using SABRE-SHEATH, J. Phys. Chem. C 119 (2015) 8786–8797, https://doi.org/10.1021/acs.jpcc.5b01799.
[22] D.A. Barskiy, R.V. Shchepin, A.M. Coffey, T. Theis, W.S. Warren, B.M. Goodson, E. Y. Chekmenev, Over 20% ^{15}N hyperpolarization in under one minute for metronidazole, an antibiotic and hypoxia probe, J. Am. Chem. Soc. 138 (26) (2016) 8080–8083, https://doi.org/10.1021/jacs.6b04784.
[23] J.-B. Hövener, S. Knecht, N. Schwaderlapp, J. Hennig, D. von Elverfeldt, Continuous re-hyperpolarization of nuclear spins using parahydrogen: theory and experiment, ChemPhysChem 15 (2014) 2451–2457, https://doi.org/10.1002/cphc.201402177.
[24] R.E. Mewis, K.D. Atkinson, M.J. Cowley, S.B. Duckett, G.G.R. Green, R.A. Green, L. A.R. Highton, D. Kilgour, L.S. Lloyd, J.A.B. Lohman, D.C. Williamson, Probing signal amplification by reversible exchange using an NMR flow system, Magn. Reson. Chem. 52 (2014) 358–369, https://doi.org/10.1002/mrc.4073.
[25] J.-B. Hövener, N. Schwaderlapp, R. Borowiak, T. Lickert, S.B. Duckett, R.E. Mewis, R.W. Adams, M.J. Burns, L.A.R. Highton, G.G.R. Green, A. Olaru, J. Hennig, D. von Elverfeldt, Toward biocompatible nuclear hyperpolarization using signal amplification by reversible exchange: quantitative in situ spectroscopy and high-field imaging, Anal. Chem. 86 (2014) 1767–1774, https://doi.org/10.1021/ac403653q.
[26] J.-B. Hövener, N. Schwaderlapp, T. Lickert, S.B. Duckett, R.E. Mewis, L.A.R. Highton, S.M. Kenny, G.G.R. Green, D. Leibfritz, J.G. Korvink, J. Hennig, D. von Elverfeldt, A hyperpolarized equilibrium for magnetic resonance, Nat. Commun. 4 (2013), https://doi.org/10.1038/ncomms3946 (art. no. 2946).
[27] D.A. Barskiy, K.V. Kovtunov, I.V. Koptyug, P. He, K.A. Groome, Q.A. Best, F. Shi, B. M. Goodson, R.V. Shchepin, M.L. Truong, A.M. Coffey, K.W. Waddell, E.Y. Chekmenev, In situ and ex situ low-field NMR spectroscopy and MRI endowed by SABRE hyperpolarization, ChemPhysChem 15 (2014) 4100–4107, https://doi.org/10.1002/cphc.201402607.
[28] T. Theis, M. Truong, A.M. Coffey, E.Y. Chekmenev, W.S. Warren, LIGHT-SABRE enables efficient in-magnet catalytic hyperpolarization, J. Magn. Reson. 248 (2014) 23–26, https://doi.org/10.1016/j.jmr.2014.09.005.
[29] P. Rovedo, S. Knecht, T. Bäumlisberger, A.L. Cremer, S.B. Duckett, R.E. Mewis, G. G.R. Green, M. Burns, P.J. Rayner, D. Leibfritz, J.G. Korvink, J. Hennig, G. Pütz, D. von Elverfeldt, J.-B. Hövener, Molecular MRI in the earth's magnetic field using continuous hyperpolarization of a biomolecule in water, J. Phys. Chem. B 120 (25) (2016) 5670–5677, https://doi.org/10.1021/acs.jpcb.6b02830.
[30] A.N. Pravdivtsev, A.V. Yurkovskaya, H. Zimmermann, H.-M. Viethd, K.L. Ivanov, Transfer of SABRE-derived hyperpolarization to spin-1/2 heteronuclei, RSC Adv. 5 (2015) 63615–63623, https://doi.org/10.1039/c5ra13808f.
[31] A.N. Pravdivtsev, A.V. Yurkovskaya, H.-M. Vieth, K.L. Ivanov, RF-SABRE: a way to continuous spin hyperpolarization at high magnetic fields, J. Phys. Chem. B 119 (43) (2015) 13619–13629, https://doi.org/10.1021/acs.jpcb.5b03032.
[32] N. Eshuis, R.L.E.G. Aspers, B.J.A. van Weerdenburg, M.C. Feiters, F.P.J.T. Rutjes, S. S. Wijmenga, M. Tessari, 2D NMR trace analysis by continuous hyperpolarization at high magnetic field, Angew. Chem. Int. Ed. 54 (2015) 14527–14530, https://doi.org/10.1002/anie.201507831.
[33] S. Knecht, A.S. Kiryutin, A.V. Yurkovskaya, K.L. Ivanov, Re-polarization of nuclear spins using selective SABRE-INEPT, J. Magn. Reson. 287 (2018) 10–14, https://doi.org/10.1016/j.jmr.2017.12.010.
[34] N.K.J. Hermkens, R.L.E.G. Aspers, M.C. Feiters, F.P.J.T. Rutjes, M. Tessari, Trace analysis in water-alcohol mixtures by continuous p-H2 hyperpolarization at high magnetic field, Magn. Reson. Chem. 56 (2018) 633–640, https://doi.org/10.1002/mrc.4692.
[35] K.V. Kovtunov, B.E. Kidd, O.G. Salnikov, L.B. Bales, M.E. Gemeinhardt, J. Gesiorski, R.V. Shchepin, E.Y. Chekmenev, B.M. Goodson, I.V. Koptyug, Imaging of biomolecular NMR signals amplified by reversible exchange with parahydrogen inside an MRI scanner, J. Phys. Chem. C 121 (2017) 25994–25999, https://doi.org/10.1021/acs.jpcc.7b10549.
[36] M. Suefke, S. Lehmkuhl, A. Liebisch, B. Blümich, S. Appelt, Para-hydrogen raser delivers sub-millihertz resolution in nuclear magnetic resonance, Nat. Phys. 13 (2017) 568–572, https://doi.org/10.1038/nphys4076.
[37] A.N. Pravdivtsev, I.V. Skovpin, A.I. Svyatova, N.V. Chukanov, L.M. Kovtunova, V. I. Bukhtiyarov, E.Y. Chekmenev, K.V. Kovtunov, I.V. Koptyug, J.-B. Hövener, Chemical exchange reaction effect on polarization transfer efficiency in SLIC-SABRE, J. Phys. Chem. A 122 (2018) 9107–9114, https://doi.org/10.1021/acs.jpca.8b07163.
[38] B.J.A. van Weerdenburg, S. Glöggler, N. Eshuis, A.H.J.T. Engwerda, J.M.M. Smits, R. de Gelder, S. Appelt, S.S. Wymenga, M. Tessari, M.C. Feiters, B. Blümich, F.P.J. T. Rutjes, Ligand effects of NHC-iridium catalysts for signal amplification by reversible exchange (SABRE), Chem. Commun. 49 (2013) 7388–7390, https://doi.org/10.1039/c3cc43423k.
[39] M. Fekete, C. Gibard, G.J. Dear, G.G.R. Green, A.J.J. Hooper, A.D. Roberts, F. Cisnetti, S.B. Duckett, Utilisation of water soluble iridium catalysts for signal amplification by reversible exchange, Dalton Trans. 44 (2015) 7870–7880, https://doi.org/10.1039/c5dt00311c.
[40] P. Spannring, I. Reile, M. Emondts, P.P.M. Schleker, N.K.J. Hermkens, N.G.J. van der Zwaluw, B.J.A. van Weerdenburg, P. Tinnemans, M. Tessari, B. Blümich, F.P. J.T. Rutjes, M.C. Feiters, A new Ir-NHC catalyst for signal amplification by reversible exchange in D_2O, Chem. A Eur. J. 22 (27) (2016) 9277–9282, https://doi.org/10.1002/chem.201601211.
[41] J.F.P. Colell, M. Emondts, A.W.J. Logan, K. Shen, J. Bae, R.V. Shchepin, J. Gerardo, X. Ortiz, P. Spannring, Q. Wang, S.J. Malcolmson, E.Y. Chekmenev, M.C. Feiters, F.P.J.T. Rutjes, B. Blümich, T. Theis, W.S. Warren, Direct hyperpolarization of nitrogen-15 in aqueous media with parahydrogen in reversible exchange, J. Am. Chem. Soc. 139 (23) (2017) 7761–7767, https://doi.org/10.1021/jacs.7b00569.
[42] L.D. Vázquez-Serrano, B.T. Owens, J.M. Buriak, Catalytic olefin hydrogenation using N-heterocyclic carbene-phosphine complexes of iridium, Chem. Commun. (21) (2002) 2518–2519, https://doi.org/10.1039/b208403a.
[43] I. Kownacki, M. Kubicki, K. Szubert, B. Marciniec, Synthesis, structure and catalytic activity of the first iridium(i) siloxide versus chloride complexes with 1,3-mesitylimidazolin-2-ylidene ligand, J. Organomet. Chem. 693 (2) (2008) 321–328, https://doi.org/10.1016/j.jorganchem.2007.11.013.
[44] K.D. Atkinson, M.J. Cowley, P.I.P. Elliott, S.B. Duckett, G.G.R. Green, J. López-Serrano, A.C. Whitwood, Spontaneous transfer of parahydrogen derived spin order to pyridine at low magnetic field, J. Am. Chem. Soc. 131 (2009) 13362–13368, https://doi.org/10.1021/ja903601p.
[45] K.D. Atkinson, M.J. Cowley, S.B. Duckett, P.I.P. Elliott, G.G.R. Green, J. López-Serrano, I.G. Khazal, A.C. Whitwood, Para-hydrogen induced polarization without incorporation of para-hydrogen into the analyte, Inorg. Chem. 48 (2009) 663–670, https://doi.org/10.1021/ic8020029.
[46] N. Eshuis, N. Hermkens, B.J.A. van Weerdenburg, M.C. Feiters, F.P.J.T. Rutjes, S. S. Wijmenga, M. Tessari, Toward nanomolar detection by NMR through SABRE hyperpolarization, J. Am. Chem. Soc. 136 (2014) 2695–2698, https://doi.org/10.1021/ja412994k.
[47] A.M. Coffey, K.V. Kovtunov, D.A. Barskiy, I.V. Koptyug, R.V. Shchepin, K.W. Waddell, P. He, K.A. Groome, Q.A. Best, F. Shi, B.M. Goodson, E.Y. Chekmenev, High-resolution low-field molecular magnetic resonance imaging of hyperpolarized liquids, Anal. Chem. 86 (2014) 9042–9049, https://doi.org/10.1021/ac501638p.
[48] A.W.J. Logan, T. Theis, J.F.P. Colell, W.S. Warren, S.J. Malcolmson, Hyperpolarization of nitrogen-15 schiff bases by reversible exchange catalysis with para-hydrogen, Chem. A Eur. J. 22 (2016) 10777–10781, https://doi.org/10.1002/chem.201602393.
[49] K.V. Kovtunov, L.M. Kovtunova, M.E. Gemeinhardt, A.V. Bukhtiyarov, J. Gesiorski, V.I. Bukhtiyarov, E.Y. Chekmenev, I.V. Koptyug, B.M. Goodson, Heterogeneous microtesla SABRE enhancement of ^{15}N NMR signals, Angew. Chem. Int. Ed. 56 (2017) 10433–10437, https://doi.org/10.1002/anie.201705014.
[50] J.F.P. Colell, A.W.J. Logan, Z. Zhou, R.V. Shchepin, D.A. Barskiy, J. Gerardo, X. Ortiz, Q. Wang, S.J. Malcolmson, E.Y. Chekmenev, W.S. Warren, T. Theis, Generalizing, extending, and maximizing nitrogen-15 hyperpolarization induced by parahydrogen in reversible exchange, J. Phys. Chem. C 121 (12) (2017) 6626–6634, https://doi.org/10.1021/acs.jpcc.6b12097.
[51] R.V. Shchepin, B.M. Goodson, T. Theis, W.S. Warren, E.Y. Chekmenev, Toward hyperpolarized ^{19}F molecular imaging via reversible exchange with parahydrogen, ChemPhysChem 18 (15) (2017) 1961–1965, https://doi.org/10.1002/cphc.201700594.
[52] A.M. Olaru, T.B.R. Robertson, J.S. Lewis, A. Antony, W. Iali, R.E. Mewis, S.B. Duckett, Extending the scope of ^{19}F hyperpolarization through signal amplification by reversible exchange in MRI and NMR spectroscopy, ChemistryOpen 7 (1) (2018) 97–105, https://doi.org/10.1002/open.201700166.
[53] M.J. Burns, P.J. Rayner, G.G.R. Green, L.A.R. Highton, R.E. Mewis, S.B. Duckett, Improving the hyperpolarization of ^{31}P nuclei by synthetic design, J. Phys. Chem. B 119 (15) (2015) 5020–5027, https://doi.org/10.1021/acs.jpcb.5b00686.
[54] A.M. Olaru, A. Burt, P.J. Rayner, S.J. Hart, A.C. Whitwood, G.G.R. Green, S.B. Duckett, Using signal amplification by reversible exchange (SABRE) to hyperpolarise ^{119}Sn and ^{29}Si NMR nuclei, Chem. Commun. 52 (2016) 14482–14485, https://doi.org/10.1039/c6cc07109k.
[55] D.A. Barskiy, K.V. Kovtunov, I.V. Koptyug, P. He, K.A. Groome, Q.A. Best, F. Shi, B. M. Goodson, R.V. Shchepin, A.M. Coffey, K.W. Waddell, E.Y. Chekmenev, The feasibility of formation and kinetics of NMR signal amplification by reversible exchange (SABRE) at high magnetic field (9.4 T), J. Am. Chem. Soc. 136 (2014) 3322–3325, https://doi.org/10.1021/ja501052p.
[56] A.N. Pravdivtsev, A.V. Yurkovskaya, H.-M. Viethc, K.L. Ivanov, Spin mixing at level anti-crossings in the rotating frame makes high-field SABRE feasible, Phys. Chem. Chem. Phys. 16 (2014) 24672–24675, https://doi.org/10.1039/c4cp03765k.
[57] L.S. Lloyd, R.W. Adams, M. Bernstein, S. Coombes, S.B. Duckett, G.G.R. Green, R. J. Lewis, R.E. Mewis, C.J. Sleigh, Utilization of SABRE-derived hyperpolarization to detect low-concentration analytes via 1D and 2D NMR methods, J. Am. Chem. Soc. 134 (2012) 12904–12907, https://doi.org/10.1021/ja3051052.
[58] I. Reile, R.L.E.G. Aspers, J.-M. Tyburn, J.G. Kempf, M.C. Feiters, F.P.J.T. Rutjes, M. Tessari, DOSY analysis of micromolar analytes: Resolving dilute mixtures by SABRE hyperpolarization, Angew. Chem. Int. Ed. 56 (31) (2017) 9174–9177, https://doi.org/10.1002/anie.201703577.
[59] N.K.J. Hermkens, M.C. Feiters, F.P.J.T. Rutjes, S.S. Wijmenga, Marco Tessari, High field hyperpolarization-EXSY experiment for fast determination of dissociation rates in SABRE complexes, J. Magn. Reson. 276 (2017) 122–127, https://doi.org/10.1016/j.jmr.2017.01.011.
[60] S.B. Duckett, R.E. Mewis, Application of parahydrogen induced polarization techniques in NMR spectroscopy and imaging, Acc. Chem. Res. 45 (8) (2012) 1247–1257, https://doi.org/10.1021/ar2003094.

[61] S. Glöggler, J. Colell, S. Appelt, Para-hydrogen perspectives in hyperpolarized NMR, J. Magn. Reson. 235 (2013) 130–142, https://doi.org/10.1016/j.jmr.2013.07.010.
[62] K.M. Appleby, R.E. Mewis, A.M. Olaru, G.G.R. Green, I.J.S. Fairlamb, S.B. Duckett, Investigating pyridazine and phthalazine exchange in a series of iridium complexes in order to define their role in the catalytic transfer of magnetisation from para-hydrogen, Chem. Sci. 6 (2015) 3981–3993, https://doi.org/10.1039/c5sc00756a.
[63] S. Glöggler, R. Müller, J. Colell, M. Emondts, M. Dabrowski, B. Blümich, S. Appelt, Para-hydrogen induced polarization of amino acids, peptides and deuterium-hydrogen gas, Phys. Chem. Chem. Phys. 13 (2011) 13759–13764, https://doi.org/10.1039/c1cp20992b.
[64] F. Shi, A.M. Coffey, K.W. Waddell, E.Y. Chekmenev, B.M. Goodson, Heterogeneous solution NMR signal amplification by reversible exchange, Angew. Chem. Int. Ed. 53 (2014) 7495–7498, https://doi.org/10.1002/anie.201403135.
[65] F. Shi, A.M. Coffey, K.W. Waddell, E.Y. Chekmenev, B.M. Goodson, Nanoscale catalysts for NMR signal enhancement by reversible exchange, J. Phys. Chem. C 119 (2015) 7525–7533, https://doi.org/10.1021/acs.jpcc.5b02036.
[66] W. Iali, A.M. Olaru, G.G.R. Green, S.B. Duckett, Achieving high levels of NMR-hyperpolarization in aqueous media with minimal catalyst contamination using SABRE, Chem. A Eur. J. 23 (44) (2017) 10491–10495, https://doi.org/10.1002/chem.201702716.
[67] A.N. Pravdivtsev, A.V. Yurkovskaya, H.-M. Vieth, K.L. Ivanov, R. Kaptein, Level anti-crossings are a key factor for understanding para-hydrogen-induced hyperpolarization in SABRE experiments, ChemPhysChem 14 (14) (2013) 3327–3331, https://doi.org/10.1002/cphc.201300595.
[68] A.S. Kiryutin, A.V. Yurkovskaya, H. Zimmermann, H. Vieth, K.L. Ivanov, Complete magnetic field dependence of SABRE-derived polarization, Magn. Reson. Chem. 56 (2017) 651–662, https://doi.org/10.1002/mrc.4694.
[69] S. Lehmkuhl, M. Wiese, L. Schubert, M. Held, M. Küppers, M. Wessling, B. Blümich, Continuous hyperpolarization with parahydrogen in a membrane reactor, J. Magn. Reson. 291 (2018) 8–13, https://doi.org/10.1016/j.jmr.2018.03.012.
[70] M. Fekete, O. Bayfield, S.B. Duckett, S. Hart, R.E. Mewis, N. Pridmore, P.J. Rayner, A. Whitwood, Iridium(III) hydrido N-heterocyclic carbene-phosphine complexes as catalysts in magnetization transfer reactions, Inorg. Chem. 52 (2013) 13453–13461, https://doi.org/10.1021/ic401783c.
[71] K.X. Moreno, K. Nasr, M. Milne, A.D. Sherry, W.J. Goux, Nuclear spin hyperpolarization of the solvent using signal amplification by reversible exchange (SABRE), J. Magn. Reson. 257 (2015) 15–23, https://doi.org/10.1016/j.jmr.2015.04.013.
[72] R.V. Shchepin, M.L. Truong, T. Theis, A.M. Coffey, F. Shi, K.W. Waddell, W.S. Warren, B.M. Goodson, E.Y. Chekmenev, Hyperpolarization of neat liquids by NMR signal amplification by reversible exchange, J. Phys. Chem. Lett. 6 (2015) 1961–1967, https://doi.org/10.1021/acs.jpclett.5b00782.
[73] S. Lehmkuhl, M. Emondts, L. Schubert, P. Spannring, J. Klankermayer, B. Blümich, P. Schleker, Hyperpolarizing water with para-hydrogen, ChemPhysChem 18 (18) (2017) 2426–2429, https://doi.org/10.1002/cphc.201700750.